Journal of Theoretical Biology 380 (2015) 309–314

Contents lists available at ScienceDirect

Journal of Theoretical Biology

journal homepage: www.elsevier.com/locate/yjtbi

Incomplete penetrance: The role of stochasticity in developmental cell colonization

Benjamin J. Binder [a,*], Kerry A. Landman [b], Donald F. Newgreen [c], Joshua V. Ross [a]

[a] School of Mathematical Sciences, University of Adelaide, South Australia 5005, Australia
[b] School of Mathematics and Statistics, University of Melbourne, Victoria 3010, Australia
[c] Murdoch Childrens Research Institute, Royal Children's Hospital, Parkville, Victoria 3052, Australia

HIGHLIGHTS

- Developmental cell colonization is modeled with two Markovian processes.
- Models include cell proliferation and motility, and gut tissue growth mechanisms.
- Probability of cell colonization success is quantified.
- Propose a new mechanism for incomplete penetrance requiring no genetic differences.
- Variability in colonization attributed to stochastic interactions of cellular mechanisms.

ARTICLE INFO

Article history:
Received 21 August 2014
Received in revised form
21 May 2015
Accepted 22 May 2015
Available online 3 June 2015

Keywords:
Markov chain model
Agent-based model
Incomplete penetrance
Hirschsprung Disease

ABSTRACT

Cell colonization during embryonic development involves cells migrating and proliferating over growing tissues. Unsuccessful colonization, resulting from genetic causes, can result in various birth defects. However not all individuals with the same mutation show the disease. This is termed incomplete penetrance, and it even extends to discordancy in monozygotic (identical) twins. A one-dimensional agent-based model of cell migration and proliferation within a growing tissue is presented, where the position of every cell is recorded at any time. We develop a new model that approximates this agent-based process – rather than requiring the precise configuration of cells within the tissue, the new model records the total number of cells, the position of the most advanced cell, and then invokes an approximation for how the cells are distributed. The probability mass function (PMF) for the most advanced cell is obtained for both the agent-based model and its approximation. The two PMFs compare extremely well, but using the approximation is computationally faster. Success or failure of colonization is probabilistic. For example for sufficiently high proliferation rate the colonization is assured. However, if the proliferation rate is sufficiently low, there will be a lower, say 50%, chance of success. These results provide insights into the puzzle of incomplete penetrance of a disease phenotype, especially in monozygotic twins. Indeed, stochastic cell behavior (amplified by disease-causing mutations) within the colonization process may play a key role in incomplete penetrance, rather than differences in genes, their expression or environmental conditions.

1. Introduction

Cell colonization during embryonic development involves cells migrating and proliferating over growing tissues. Unsuccessful colonization can result in various birth defects. For example, in the case of the neural crest (Zhang et al., 2014), failure of colonization in the enteric nervous system may lead to Hirschsprung Disease (Newgreen and Young, 2002) and failure in cranial–facial development may lead to cleft lip and palate (Muhamad and Azzaldeen, 2012; Parsons et al., 2008). In these conditions the colonizing cell population fails to populate the entire field (which is itself growing), or fails to provide the normal number of cells.

There are many genetic causes of these diseases and these are often classed as dominant mutations. However not all individuals with the same mutation show the disease; this is termed incomplete penetrance. This incomplete penetrance extends even to discordancy in monozygotic (identical) twins.

Most explanations of incomplete penetrance in genetically identical individuals are made by assuming differences in gene

* Corresponding author. Tel.: 61 883133244.
E-mail address: benjamin.binder@adelaide.edu.au (B.J. Binder).

http://dx.doi.org/10.1016/j.jtbi.2015.05.028
0022-5193/

expression between affected and unaffected individuals. The work presented here suggests a novel explanation of incomplete penetrance which is based on stochastic cell behavior, amplified by disease-causing mutations.

We investigate the success or otherwise of a colonization process by considering two continuous-time one-dimensional Markovian models: one an agent-based model and the other an approximating model. The agent-based (cellular automata) model is based on a 2-dimensional discrete-time model which has been used previously to simulate the invasion of NC cells within the growing gut tissue (Binder et al., 2008; Binder and Landman, 2009; Simpson et al., 2007; Zhang et al., 2010). Here we use the continuous-time 1-D analog of that model.

Although the probability distribution of the state of this agent-based model is determined by a set of ordinary differential equations, the size of this system makes it impractical to solve. We therefore derive a second model which is a Markov chain approximation to quantify more efficiently the variability of the cell invasion front, providing a measure of colonization success.

The approximation is validated by comparison with averaged simulation data from the agent-based model of the overall process, demonstrating a high level of accuracy across a wide range of parameter space.

2. Agent-based model

We consider a continuous-time one-dimensional discrete-state agent-based model to simulate a cell colonization process. All quantities and variables are non-dimensional. The domain (tissue) is a single row of lattice sites whose positions are located at the discrete integer points $x = 1, 2, \ldots, L(t)$, where $L(t)$ is the length of the domain that elongates with time t. Each lattice site of the domain can be either occupied by a single agent or unoccupied. The total number of agents at any given time is $N(t) \in \{1, 2, \ldots, L(t)\}$. The local rules for domain growth, agent motility and agent proliferation events are similar to those described previously (Binder et al., 2008; Binder and Landman, 2009), and are shown in Fig. 1(a)–(c). If the target site is occupied for any motility or proliferation event, then that event is aborted. These events are volume exclusion processes (Chowdhury et al., 2005; Simpson et al., 2009). Note that if the chosen lattice site is occupied by an agent in the case of a domain growth event, then the agent is transported to the right with the moving lattice site.

The model is updated in continuous-time (Gillespie, 1977) with domain growth rate λ_g, agent motility rate λ_m, and proliferation rate λ_p. We define the propensity function as $\lambda = (\lambda_m + \lambda_p)N(t) + \lambda_g L(t)$, giving the total rate at which events occur at time t. Random numbers are drawn from the exponential distribution and uniform distribution as $E[\lambda^{-1}]$ and $U[0, 1]$, respectively. The algorithm then proceeds as follows, being terminated at either a maximum chosen time $t_f > 0$ or maximum chosen domain length $L_f > L(0)$.

Step 1: Calculate the propensity function λ given the current state, and update the time with $t := t + E[\lambda^{-1}]$. If $t < t_f$ (or alternatively $L(t) < L_f$) go to *Step* 2; else stop.
Step 2: Generate a random number $R = \lambda U[0, 1]$.
Step 3: Decide which type of event to perform. If $R < \lambda_m N(t)$ then attempt to perform a motility event. If $\lambda_m N(t) \le R < (\lambda_m + \lambda_p)N(t)$ then attempt to perform a proliferation event. If $R \ge (\lambda_m + \lambda_p)N(t)$ then perform a domain growth event. Update the state as appropriate.
Step 4: If $t < t_f$ (or alternatively $L(t) < L_f$) repeat *Steps* 1–3; else stop.

We initialize a simulation by populating all the lattice sites to the left of and including the site z_0, where $1 \le z_0 \le L(0)$, and then record the position of the rightmost agent at later times. This provides a measure for the cell invasion front. Shown in Fig. 1(d)–(f) is a simulation that was terminated when $L_f = 12$, with $z_0 = 2$, $L(0) = 4$, $\lambda_m = \lambda_p = 0.5$ and $\lambda_g = 0.1$.

To quantify the success of the colonization, we record the counts (number of occurrences) of the positions $z(t)$, where $z_0 \le z(t) \le L(t)$ for $t > 0$ and $z(0) = z_0$, of the rightmost or leading agents from M realizations. Dividing the counts by the number of simulations M then produces an estimated probability mass function (PMF) $P(z)$, for the position of the rightmost agent or invasion front; that is, $P(z)$ is the probability that the right-most agent is in position z at the stopping time. Typical PMFs are shown in Figs. 2 and 3 (light gray). We delay the discussion of these curves to Section 4. In particular, we define a successful invasion as one in which the right-most (most advanced) cell occupies a site in the last fraction $(1-\beta)$ of sites. As such, we evaluate and report the *probability of success* by the sum, Q, of marginal probabilities of occupancy $P(z)$ in the last fraction $(1-\beta)$ of sites

$$Q = \sum_{z = \lfloor \beta L_f \rfloor}^{L_f} P(z).$$

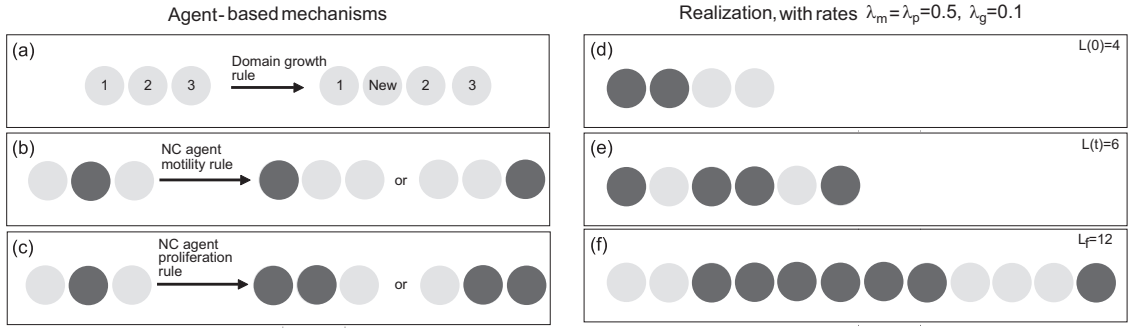

Fig. 1. Agent-based mechanisms and typical realization. (a)–(c) Agent-based mechanisms, domain agents (light gray) and agents (dark gray). (a) Domain growth rule. A domain agent is randomly selected to proliferate. After mitotic division the selected agent, and all the agents to its right, are transported one agent-length to the right. A new agent is inserted in the original position of the agent that was selected to proliferate. (b) Agent motility rule. The agent can move to one of the two configurations shown with equal probability. (c) Agent proliferation rule. The mother agent divides into two daughter agents. After mitotic division two possible configurations can occur with equal probability. (d)–(f) Typical realization, with $\lambda_m = \lambda_p = 0.5$ and $\lambda_g = 0.1$. (d) Initial condition, $z_0 = 2$ and $L(0) = 4$. (e) Snapshot at domain length $L(t) = 6$. (f) The simulation was terminated at the chosen domain length $L_f = 12$.

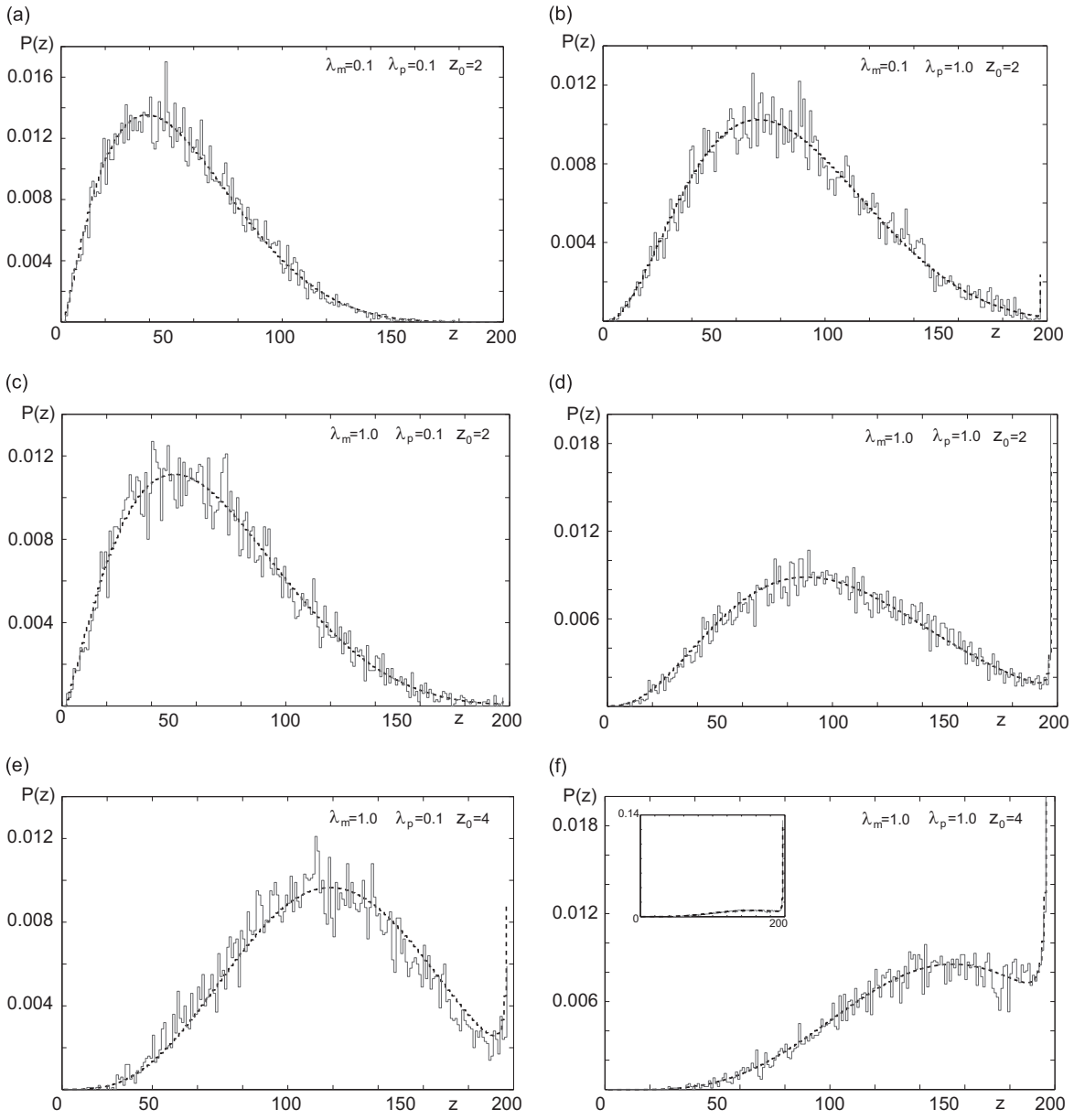

Fig. 2. Comparison of PMFs for the position of the rightmost (leading) agent generated by the agent-based model and the Markov chain approximation for various values of motility rate λ_m, proliferation rate λ_p and initial position of the rightmost agent z_0. The agent-based model results (gray) are generated from $M = 10,000$ simulations with a final length $L_f = 197$ and average final time $\overline{t} = 8$; $L(0) = 8$ and $\lambda_g = 0.4$. The Markov chain approximation is also shown (the black broken curves). (a) Initial population $z_0 = 2$; $\lambda_m = 0.1$; $\lambda_p = 0.1$. (b) Initial population $z_0 = 2$; $\lambda_m = 0.1$; $\lambda_p = 1$. (c) Initial population $z_0 = 2$; $\lambda_m = 1.0$; $\lambda_p = 0.1$. (d) Initial population $z_0 = 2$; $\lambda_m = 1.0$; $\lambda_p = 1.0$. (e) Initial population $z_0 = 4$; $\lambda_m = 1.0$; $\lambda_p = 0.1$. (f) Initial population $z_0 = 4$; $\lambda_m = 1.0$; $\lambda_p = 1.0$. The inset shows the complete data.

3. Markov chain approximation

We now consider an approximating Markov chain model of the process of cell invasion and tissue growth. We define the model and then discuss the evaluation of the main quantity of interest, the PMF of rightmost agent.

Our approximating model is a trivariate continuous-time Markov chain, where the variables are $z(t)$, the position of the rightmost occupied site, $n(t)$, the number of sites occupied to the left of the rightmost occupied site, and $l(t)$, the length of tissue, at time t.

Since agents cannot jump over each other in the model, the agent in the rightmost position will be the same agent, or a daughter of the agent, in the rightmost position for all t. This rightmost agent can move to the right, via motility and proliferation, uninhibited provided it is currently not occupying the last site in the tissue, and hence requires no approximation. However, an approximation is required when modeling motility and proliferation of this agent when moving to the left, and for the motility and proliferation of the other $n(t)$ agents, as we do not (typically) know the exact configuration of the agents and hence the exact probability the sites will be vacant, and hence accessible for movement and proliferation events. Tissue growth can also be modeled without approximation; however, its effect on the configuration of the $n(t)$ agents is undetermined.

The dynamics (non-zero transition rates) of our model are described by six changes of state, detailed below

(i) $(z,n,l) \to (z+1,n,l)$ at rate $\frac{\lambda_m}{2} 1_{\{z<l\}}$

(ii) $(z,n,l) \to (z+1,n+1,l)$ at rate $\frac{\lambda_p}{2} 1_{\{z<l\}}$

(iii) $(z,n,l)\to(z-1,n,l)$ at rate $\frac{\lambda_m}{2}b(z,n)$

(iv) $(z,n,l)\to(z,n+1,l)$ at rate $\frac{\lambda_p}{2}(n+1)b(z,n)$

(v) $(z,n,l)\to(z+1,n,l+1)$ at rate $\lambda_g z$

(vi) $(z,n,l)\to(z,n,l+1)$ at rate $\lambda_g(l-z)$.

Here the notation $1_{\{z<l\}}$ is unity if $z<l$ and zero otherwise. The $b(z,n)$ is used to approximate the probability of a randomly selected site being vacant and is defined as

$$b(z,n)=\frac{(z-n-1)}{(z-1)}\frac{1}{\left[1+\frac{\epsilon n}{(\lambda_m+1)}\right]},$$

where ϵ is a parameter that must be selected.

Transition (i) describes a motility event of the rightmost agent to its immediate right (to $z+1$), while (ii) describes a proliferation event of the rightmost agent, where a daughter is placed to its immediate right ($z+1$). Only the second event changes the total number of agents to the left of the rightmost agent, and the length of the domain remains unchanged. In both these cases, we know that $z+1$ is unoccupied, so the transitions automatically occur. Transitions (v) and (vi) represent domain growth to the left and right of the rightmost agent respectively.

Transitions (iii) and (iv) involve additional terms which are approximations requiring explanation. The first, (iii), represents a move of the rightmost agent to its immediate left (to $z-1$) with no change in the number of agents. The second, (iv), represents a proliferation event of the rightmost agent at z to its immediate left ($z-1$) or a proliferation event of any of the n agents to the left of z, ensuring that the rightmost agent remains at z, but the total number of agents increases by unity. A movement or proliferation event can only occur if the neighboring site is unoccupied, so depends on volume exclusion. We therefore need to modify the attempted transition rate (namely $\lambda_m/2$ in (iii) and $\lambda_p/2$ in (iv)) by an approximation to the probability of a randomly selected site being vacant, which we denoted as $b(z,n)$.

The form of approximation was chosen as follows: it is a probability, so must take values between 0 and 1. In particular, if there were no occupied sites then the probability should theoretically be 1, and when the lattice is full (corresponding to $n=z-1$) then the probability should be 0. Furthermore, if the occupied sites were distributed uniformly at random, between sites 1 and the rightmost occupied site z, then the probability is $(z-n-1)/(z-1)$ (since it is just the number of vacant sites to the left of the rightmost agent divided by the total number of sites to its left). However, due to the nature of the proliferation mechanism of the process, it is more likely that occupied sites will form clusters, hence decreasing this probability from that corresponding to a uniform distribution. This is achieved for $\epsilon>0$; but note that as $\lambda_m\to\infty$ for a fixed ϵ and n, the function $b(z,n)$ approaches the uniformly-distributed probability, which is expected as motility increases. Throughout we fix $\epsilon=0.075$, which was chosen to provide a close match to simulations across a large number of parameter combinations. We note that this approximation is *ad hoc*, and that a more rigorous derivation of an approximation of this ilk might be possible, for example via the use of closure approximations (Hiebeler, 1997; Baker and Simpson, 2010).

We evaluate the full distribution of the state of this approximating Markov chain by solving the forward equation using `EXPOKIT` (Sidje, 1998). From this distribution we may evaluate any quantity of interest, such as the marginal PMF of the position of the rightmost agent shown by the broken curves in Figs. 2 and 3. Note, that in the case of Fig. 3, we must truncate the state space by imposing a maximum length L_T; we used $L_T=450$. This is compared with an estimate based upon 10,000 simulations.

However, in the case of evaluating the probability of success, Q, we may adopt a more computationally-efficient approach. We are simply evaluating the hitting probability of the set of states $\{\lfloor\beta L_f\rfloor,\ldots,L_f\}$, and hence may be evaluated by solving a system of linear equations (see Theorem 3.3.1 of Norris (1997)). To solve this system of linear equations efficiently, we used MATLAB's preconditioned `bicgstab` algorithm, which implements a biconjugate gradient (stabilized) method with an incomplete LU-factorization as a preconditioner.

4. Results and discussion

PMFs of the rightmost agent have been generated with the two different stopping criteria (either a final length L_f or a final time t_f is chosen), for various values of the motility rate λ_m, proliferation rate λ_p and the initial position of the rightmost agent z_0.

When the colonization process is terminated at a fixed domain length $L_f=197$, with an average time of simulation $\bar{t}=8$ (Fig. 2), the effect of increasing λ_m, λ_p or z_0 is an increase in colonization success, indicated by the probability distribution of the position of the advancing colonization front. The spikes in the PMFs (Fig. 2(b), (d)–(f)) at $L_f=197$ correspond to agents that happened to reach the end of the domain during the simulations and then being transported by the domain growth mechanism.

Alternatively, when the colonization process is terminated at a fixed time $t_f=8$, with an average final length of domain $\bar{L}_f=197$ (Fig. 3), we observe that there is a smaller increase in the advancing colonization front (Fig. 3) for the same increase in

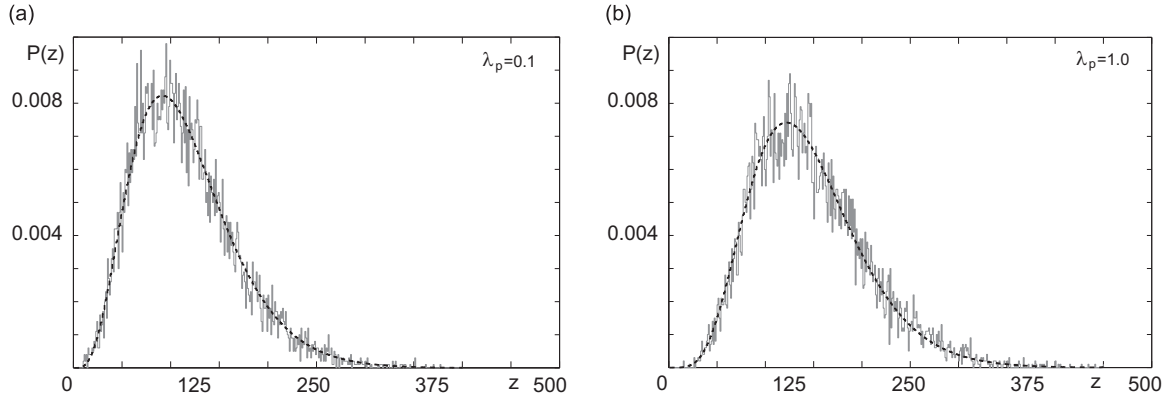

Fig. 3. Comparison of PMFs generated by the agent-based model and the Markov chain approximation for various values of proliferation rate λ_p. The agent-based model results (gray) are generated from $M=10,000$ simulations with a final length time $t_f=8$ and average final length $\bar{L}=197$; $L(0)=8$, $z_0=4$, $\lambda_m=1.0$ and $\lambda_g=0.4$. The Markov chain approximation is also shown (the black broken curves). (a) $\lambda_p=0.1$. (b) $\lambda_p=1.0$.

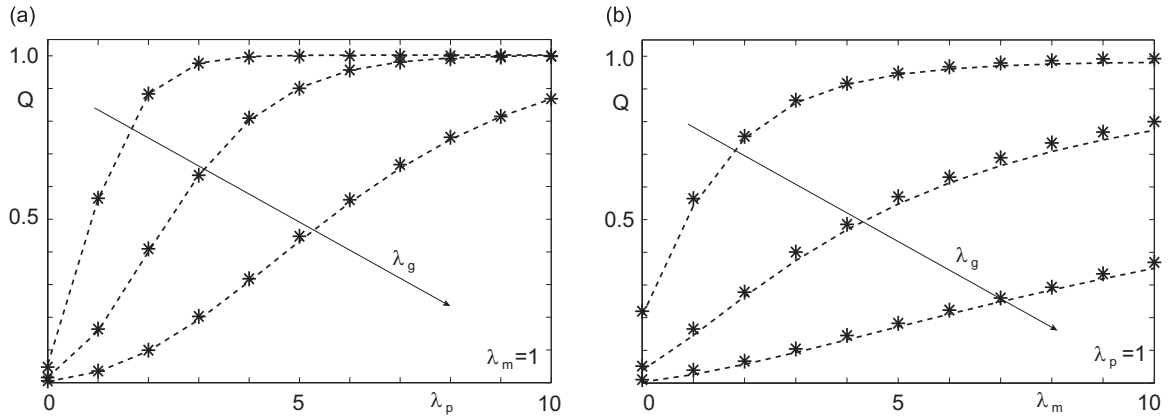

Fig. 4. Sum of probabilities Q, in the last 25% of the length of tissue, $L_f = 197$, $L(0) = 8$ and $z_0 = 2$. The arrow indicates the increasing rate of tissue growth for the three sets of results, $\lambda_g = \{0.2, 0.4, 0.8\}$. The agent-based model, averaged over $M = 10,000$ simulations (black markers), and the Markov chain approximation (broken curves) are both illustrated. (a) Increasing proliferation rate with fixed motility rate; $\lambda_m = 1$. (b) Increasing motility rate with fixed proliferation rate; $\lambda_p = 1$.

proliferation rate of that in the fixed final length case (Fig. 2(e) and (f) with the same parameter values). Also noteworthy, the spikes in the PMFs are no longer present in Fig. 3, due to the (large) variability in the final length of the domain.

Moreover, the comparison between the averaged simulation data (light gray curves) and Markov chain approximation (black broken curves) for both sets of results is excellent. Therefore, our approximate Markov chain is a good approximation to the agent-based model.

In Fig. 4 we chose $\beta = 3/4$ for the case where a given L_f is the stopping criteria, and investigate a wide region of parameter space, noting that the relative values of motility and proliferation are only relevant in Fig. 4. The effect of increasing both the proliferation and motility rates (λ_p and λ_m respectively), for three values of the tissue growth rate (λ_g) is illustrated. Note that as the value of $\beta \to 1^-$, the curves will increase at a less rapid rate.

Comparison between Fig. 4(a) and (b) shows that the probability of success, Q, increases more rapidly as the agent proliferation rate, λ_p, is increased than when the agent motility rate, λ_m, is increased. Indeed the results suggest that increasing the proliferation is the most effective way of decreasing the probability of failure to complete colonization for a fixed tissue growth rate, consistent with previous findings (Zhang et al., 2010).

There are computational advantages in using the approximation over the full simulations. To produce the Q results in Fig. 4, the evaluation based upon the approximation took significantly less time than the direct simulation method – approximately one quarter of the time (estimates based upon 10,000 realizations and using MATLAB R2013b on a Macintosh with 3Ghz 8-Core Intel Xeon E5 processor and 64GB of RAM). The time to evaluate Q using the approximation is independent of the rates of domain growth, λ_g, motility rate, λ_m, and proliferation rate, λ_p, whereas estimation using simulation increases in computation time as domain growth, λ_g, decreases (as it takes longer to reach the maximum domain length), and as motility, λ_m, and proliferation, λ_p, increase (there exists more events per unit time), with motility appearing to have a larger impact on increasing the computation time.

The precise requirements for successful colonization are unclear. The definition we have used is one potential requirement, and one that has benefits in terms of allowing for a simplified model leading to more computationally-efficient and accurate assessment. However, any sensible choice of a potential requirement is likely to result in qualitatively similar curves to those presented in Fig. 4, and hence supports the overall conclusions of the paper: that stochasticity will be important to success or otherwise of colonization and may be an important component of incomplete penetrance.

In the one-dimensional model, cells are unable to pass each other. This reduces the complexity of problem considerably. Whilst a two-dimensional approximation could be specified following the same logic used here, this would require a much larger state space. In particular, in two dimensions the state would need to record the position of the right-most cell and the total number of cells to its right in every row. Hence, due to this curse of dimensionality, it would quickly become infeasible to handle numerically the analysis of the problem in two dimensions.

The results in Fig. 4 have biological implications to incomplete penetrance, where not all individuals with the same mutation show the disease or show variable severity. The most puzzling aspect of incomplete penetrance occurs when monozygotic (identical) twins are discordant. These surprising variations have been discussed since the mid-1920s with their biology receiving renewed interest (Oates, 2011).

Hirschsprung Disease (Hannon, 1988; Moore et al., 1979; Siplovich et al., 1983) and facial and cardiac neurocristopathies (Lu et al., 2001; Muhamad and Azzaldeen, 2012; Parsons et al., 2008) illustrate this phenomena. For example, in a description of over 130 cases of Hirschsprung Disease, Jung (1995) noted three sets of monozygotic twins, all of whom were discordant. Moreover, in another set of monozygotic twins, Hirschsprung Disease occurred with sensorineural deafness. This association (Waardenburg Syndrome type 4 or Waardenburg–Shah syndrome) arises from mutations in genes (SOX10, EDNRB or EDN3) that control development of both the ENS and the auditory system. However, in these twins, both had deafness but only one had Hirschsprung Disease.

Incomplete penetrance of a disease phenotype is usually explained by assuming that, between individuals with the same primary disease-causing mutation, other pre-existing differences occur which determine the difference in disease phenotype. In individuals with different genotypes, this difference in disease expression is assumed to occur mostly because individuals have different alleles of so-called disease modifier genes (Nadeau, 2003). Indeed, a number of genes that modify the penetrance of Hirschsprung Disease genes have been described (Wallace and Anderson, 2011). In highly inbred animals or monozygotic twins each individual has the same modifier gene variants, yet reduced penetrance disease still occurs. In this case, the first assumption is that differences occur even between such closely related individuals in the gestational or post-gestational environment, and this differentially influences gene expression (Khoury et al., 1988). The second assumption is that differences in expression of genes that influence the specific phenotype can arise between individuals by somatic genetic or epigenetic mutations. These two effects can

interact in a complex way (Gordon et al., 2012). In any case, although these genetic differences may arise stochastically, once present they drive the phenotype so that some individuals are affected while others with the same primary disease-causing mutation are not. In theory at least these gene sequence or expression differences, or epigenetic differences, can be discovered by large scale genetic testing (Grundberg et al., 2012).

We propose here an additional and fundamentally different mechanism for incomplete penetrance which requires no differences of genes or their expression, or change of environmental conditions. Our models show that there exists identical starting conditions with a variable success in colonization, hence allowing for incomplete penetrance. For example, if the cells has sufficiently low proliferation rate λ_p caused by disease-causing mutations, then from Fig. 4(a), we observe that there exists conditions whereby there is a lower, say 50%, chance of colonization success. This may be the situation for discordant monozygotic twins. This explanation depends on the rules that govern defined aspects of the behavior of individual cells having innately stochastic components, in this case their proliferation and movement (Young et al., 2014). This model could apply to many incompletely penetrant birth defects, particularly neural crest disorders (Breckpot et al., 2011; Newgreen and Young, 2002; Singh et al., 2002). This means that in neural crest disorders prognostic certainty at an individual level cannot be obtained even if all determinants are known, and adds to the considerable difficulties in risk assessment for diseases with incomplete penetrance (Emery, 1986).

Acknowledgments

The contributions of Binder, Landman and Newgreen were supported by the National Health and Medical Research Council. The contribution of Ross was supported by an Australian Research Council Future Fellowship (ARC FT130100254). MCRI facilities are supported by the Victorian Governments Operational Infrastructure Support Program.

References

Baker, R.E., Simpson, M.J., 2010. Correcting mean-field approximations for birth–death movement processes. Phys. Rev. E 82, 041905.
Binder, B.J., Landman, K.A., Simpson, M.J., Mariani, M., Newgreen, D.F., 2008. Modeling proliferative tissue growth a general approach and an avian case study. Phys. Rev. E 78, 031912.
Binder, B.J., Landman, K.A., 2009. Exclusion processes on a growing domain. J. Theor. Biol. 259, 541–551.
Breckpot, J., Thienpont, B., Gewillig, M., Allegaert, K., Vermeesch, J.R., Devriendt, K., 2011. Differences in copy number variation between discordant monozygotic twins as a model for exploring chromosomal mosaicism in congenital heart defects. Mol. Syndromol. 2, 81–87.
Chowdhury, D., Schadschneider, A., Nishinari, K., 2005. Physics of transport and traffic phenomena in biology: from molecular motors and cells to organisms. Phys. Life Rev. 2, 318–352.
Emery, A.E.H., 1986. Risk estimation in autosomal dominant disorders with reduced penetrance. J. Med. Genet. 23, 316–318.
Gillespie, D.M., 1977. Exact stochastic simulation of coupled chemical reactions. J. Phys. Chem. 81, 2340–2361.
Gordon, L., et al., 2012. Neonatal DNA methylation profile in human twins is specified by a complex interplay between intrauterine environmental and genetic factors, subject to tissue-specific influence, Genome Res. 22, 1395–1406.
Grundberg, E., et al., 2012. Multiple Tissue Human Expression Resource (MuTHER) consortium mapping cis- and trans-regulatory effects across multiple tissues in twins. Nat. Genet. 44, 1084–1089.
Hannon, R.J., Boston, V.E., 1988. Discordant Hirschsprung's disease in monozygotic twins: a clue to pathogenesis?. J. Pediatr. Surg. 23, 1034–1035.
Hiebeler, D., 1997. Stochastic spatial models: from simulations to mean field and local structure approximations. J. Theor. Biol. 187, 307–319.
Jung, P.M., 1995. Hirschsprung Disease: one surgeon's experience in one institution. J. Pediatr. Surg. 30, 646–651.
Khoury, M.J., Flanders, W.D., Beaty, T.H., Optiz, J.M., 1988. Penetrance in the presence of genetic susceptibility to environmental factors. Am. J. Med. Genet. 29, 397–403.
Lu, J.H., Chung, M.Y., Hwang, B., Chien, H.P., 2001. Monozygotic twins with chromosome 22q11 microdeletion and discordant phenotypes in cardiovascular patterning. Pediatr. Cardiol. 22, 260–263.
Moore, T.C., Landers, D.B., Lachman, R.S., Ament, M.E., 1979. Hirschsprung Disease discordant in monozygotic twins: a study of possible environmental factors in the production of colonic aganglionosis. J. Pediatr. Surg. 14, 158–161.
Muhamad A.H., Azzaldeen, A., 2012. Genetic of Non-syndromic Cleft Lip and Palate, vol. 1, p. 510. doi:10.4172/scientificreports.510.
Nadeau, J.H., 2003. Modifier genes and protective alleles in humans and mice. Curr. Opin. Genet. Dev. 13, 290–295.
Newgreen, D., Young, H.M., 2002. Enteric nervous system: development and developmental disturbances—part 1. Pediatr. Dev. Pathol. 5, 224–247.
Norris, J.R., 1997. Markov Chains. Cambridge University Press, Cambridge.
Oates, A.C., 2011. What's all the noise about developmental stochasticity? Development 138, 601–607.
Parsons, T.E., Kristensen, E., Hornung, L., Diewert, V.M., Boyd, S.K., German, R.Z., Hallgrmsson, B., 2008. Phenotypic variability and craniofacial dysmorphology: increased shape variance in a mouse model for cleft lip. J. Anat. 212, 135–143.
Sidje, R.B., 1998. EXPOKIT: a software package for computing matrix exponentials. ACM Trans. Math. Softw. 24, 130–156.
Simpson, M.J., Zhang, D.C., Mariani, M., Landman, K.A., Newgreen, D.F., 2007. Cell proliferation drives neural crest cell invasion of the intestine. Dev. Biol. 302, 553–568.
Simpson, M.J., Landman, K.A., Hughes, B.D., 2009. Multi-species simple exclusion processes. Phys. A 388, 399–406.
Singh, S.M., Murphy, B., O'Reilly, R., 2002. Monozygotic twins with chromosome 22q11 deletion and discordant phenotypes: updates with an epigenetic hypothesis. J. Med. Genet. 39, e71.
Siplovich, L., Carmi, R., Bar-Ziv, J., Karplus, M., Mares, A.J., 1983. Discordant Hirschsprung Disease in monozygotic twins. J. Pediatr. Surg. 18, 639–640.
Wallace, A.S., Anderson, R.B., 2011. Genetic interactions and modifier genes in Hirschsprung's disease. World J. Gastroenterol. 17, 4937–4944.
Young, H.M., Bergner, A.J., Simpson, M.J., McKeown, S.J., Hao, M.M., Anderson, C.R., Enomoto, H., 2014. Colonizing while migrating: how do individual enteric neural crest cells behave? BMC Biol. 12, 23.
Zhang, D., Brinas, I.M., Binder, B.J., Landman, K.A., Newgreen, D.F., 2010. Neural crest regionalization for enteric nervous system formation: implications for Hirschsprung's disease and stem cell therapy. Dev. Biol. 339, 280–294.
Zhang, D., Ighaniyan, S., Stathopoulos, L., Rollo, B., Landman, K.A., Hutson, J., Newgreen, D., 2014. The neural crest: a versatile organ system. Birth Defects Res. C 102, 275–298.